

# Possible Transit Timing Variations of the TrES-3 Planetary System

Ing-Guey Jiang<sup>1</sup>, Li-Chin Yeh<sup>2</sup>, Parijat Thakur<sup>3</sup>, Yu-Ting Wu<sup>1</sup>, Ping Chien<sup>1</sup>, Yi-Ling Lin<sup>1</sup>,  
Hong-Yu Chen<sup>1</sup>, Juei-Hwa Hu<sup>1</sup>, Zhao Sun<sup>4,5</sup>, Jianghai Ji<sup>4</sup>

<sup>1</sup>*Department of Physics and Institute of Astronomy,  
National Tsing-Hua University, Hsin-Chu, Taiwan*

<sup>2</sup>*Department of Applied Mathematics,  
National Hsinchu University of Education, Hsin-Chu, Taiwan*

<sup>3</sup>*Applied Physics Unit, Department of Basic Sciences & Humanities, Guru Ghasidas  
Central University, Bilaspur (C.G.) - 495 009, India*

<sup>4</sup>*Purple Mountain Observatory, Chinese Academy of Sciences, Nanjing 210008, P.R. China*

<sup>5</sup>*Graduate School of Chinese Academy of Sciences, Beijing 100049, P.R. China*

## ABSTRACT

Five newly observed transit light curves of the TrES-3 planetary system are presented. Together with other light curve data from literature, 23 transit light curves in total, which cover an overall timescale of 911 epochs, have been analyzed through a standard procedure. From these observational data, the system's orbital parameters are determined and possible transit timing variations are investigated. Given that a null transit-timing-variation produces a fit with reduced  $\chi^2=1.52$ , our results agree with previous work, that transit timing variations might not exist in these data. However, a 1-frequency oscillating transit-timing-variation model, giving a fit with a reduced  $\chi^2=0.93$ , does possess a statistically higher probability. It is, thus, concluded that future observations and dynamical simulations for this planetary system will be very important.

*Subject headings:* planetary systems, stars: individual: TrES-3, techniques: photometric

## 1. Introduction

The development of research in extra-solar planetary systems has been successful for nearly two decades. In addition to the steadily increasing number of newly detected systems, many new discoveries of planetary properties also make this field extremely exciting. The

Doppler-shift method makes many extra-solar planetary systems known to us. The methods of transit, micro-lensing and direct imaging, also produce fruitful results. Particularly, more than 100 extra-solar planets (exoplanets) have been found to transit their host stars. Recently, based on the transit method, the Kepler space telescope has revealed many interesting results. For example, one of the greatest achievement is the discovery of a system with six planets (Lissauer et al. 2011). These results truly demonstrate the state-of-the-art power of the transit technique.

Among these detected planetary systems, TrES-3 (O’Donovan et al. 2007) attracts much attention due to its strong transit signal and short orbital period. For example, Sozzetti et al. (2009) presented a work which combines the data from spectroscopic and photometric observations of TrES-3 to obtain the best models for the host star and planet. On the other hand, Fressin et al. (2010) used the Spitzer Space Telescope to monitor TrES-3 during its secondary eclipse. The most important constraint from these results is to show that the orbital eccentricity is very small, i.e.  $|e \cos(\omega)| < 0.0056$ , where  $e$  is the orbital eccentricity and  $\omega$  is the longitude of the periastron. Furthermore, the 10.4 m Gran Telescopio Canarias (currently the world’s largest optical telescope) has obtained extremely high-precision narrow-band transit data for the TrES-3 system (Colon et al. 2010). There is almost no deviation for the data on the light curve, so this data could show a strong constraint on orbital parameters of the exoplanet TrES-3b.

In order to study the perturbation from small unknown planets and to constrain the overall orbital configuration in planetary systems, transit timing variations (TTVs) have been seriously investigated in recent years (Agol et al. 2005, Holman et al. 2005). Some of these works find that there is no TTV for the systems they studied. For example, Miller-Ricci et al. (2008) showed that there is no TTV signal above 80 s in the HD209458 system. Winn et al. (2009) also failed to confirm any TTV for the WASP-4 system. In contrast, Maciejewski et al. (2010) reported a successful case where a periodical TTV was found and, which was likely due to an additional 15 Earth-Mass planet located near the outer 1:2 mean-motion resonance in the WASP-3 system. Moreover, Holman et al. (2010) confirmed TTVs in the double transiting planetary system Kepler-9.

For the TrES-3 system, there are also many studies on TTV measurements. In addition to providing the best model for the central star and planet, Sozzetti et al. (2009) also found that the timing data gives a reduced  $\chi^2$  of about 5.87 with the assumption of no TTV. Authors concluded that there could be two possibilities: (1) the period is not a constant and, thus, it indicates some level of TTVs, or (2) the error bars might have been underestimated. Gibson et al. (2009) showed that the reduced  $\chi^2$  is 2.34 when the period is set to be a constant. They also used the data to set the mass limit of the additional planet by some

three-body simulations. Finally, Lee et al. (2011) obtained a reduced  $\chi^2$  at about 2.48 for a linear fit with a constant period.

These results imply that further studies are necessary to address the significance of TTVs and explore a possible dynamical interpretation. Thus, in this paper, we plan to do further investigations for the TrES-3 system through a self-consistent procedure with both newly obtained observational data and those from published papers. It is the first time for the TrES-3 planetary system when 23 light curves, which cover a timescale of 911 epochs, are employed to determine orbital parameters and mid-transit times through a uniform procedure. The observational results are presented in §2, the analysis of light curves is shown in §3, the comparisons with previous works are in §4, the possible TTV frequencies and models are discussed in §5 and finally the conclusions are presented in §6.

## 2. Observational Data

### 2.1. Observations and Data Reduction

In this project, we monitor the TrES-3 system with the 0.8 m telescope at Tenagra Observatory in Arizona, USA. In May and June 2010, five runs of transit observations were successfully completed by our group. For all these observations, the R band was chosen and the exposure time was set to 100 s. The field of view was 14.8 arcmin by 14.8 arcmin, giving a scale of 0.87 arcsec/pixel. The images had a typical full width at half maximum (FWHM) of 2.5 pixels. A summary of the observations is presented in Table 1.

Run	UT Date	Interval (JD-2455000)	No. of Images	Airmass Range	oot rms
1	2010 May 25	341.778 - 341.951	99	1.16-1.08	0.0019
2	2010 Jun 11	358.799 - 358.938	80	1.02-1.18	0.0020
3	2010 Jun 15	362.716 - 362.856	80	1.17-1.02	0.0025
4	2010 Jun 19	366.654 - 366.776	70	1.44-1.02	0.0018
5	2010 Jun 28	375.779 - 375.917	77	1.01-1.29	0.0021

Table 1: The log of observations of this work. For each run, the UT date, observational interval, number of exposures, airmass range and out-of-transit root-mean-square (oot rms) are listed.

Using the standard IRAF software, images were first debiased and flat-fielded, and then the differential photometry was performed. We searched for nearby bright stars with known identities to be the candidates for comparison stars. There were four candidates,

but two of them were not suitable due to the observed stellar flux being saturated or being variable. Thus, we finally used the star TYC3089-883-1 and the star TYC3089-1137-1 as our comparison stars. The flux of TrES-3 was divided by the flux of each comparison star, and also divided by the sum of the flux from both stars, to obtain three light curves. The one with the smallest out-of-transit root-mean-square was used as the TrES-3 light curve for each transit event. The values of the out-of-transit root-mean-square (oot rms) of five transit light curves are listed in Table 1, which quantify the quality of the light curves. The normalized relative flux and residuals as a function of the time of five transit light curves obtained from our observations are shown in Figure 1.

## 2.2. Other Observational Data from Literature

Eight light curves from Sozzetti et al.(2009), nine light curves from Gibson et al. (2009) and the transit data from Colon et al. (2010), which employed the 10.4 m telescope, Gran Telescopio Canarias (GTC), are included in our analysis. *Please note that we do not simply use the mid-transit times written in these papers, but analyze photometric data with the same procedure and software to do parameter fitting in a consistent way.* This approach is a better procedure to study possible TTVs when different sources of data are considered.

## 3. The Analysis of Light Curves

The Transit Analysis Package (TAP) described by Gazak et al. (2011) was used for our light-curve analysis. In addition to Gazak et al. (2011), Fulton et al. (2011) also presented the procedure of using TAP in their study of a HAT-P-13 system. The Markov Chain Monte Carlo (MCMC) technique and the model from Mandel & Agol (2002) were employed to fit the light curves in TAP. A description for other details of techniques about TAP can be found in the study by Fulton et al. (2011).

Mandel & Agol (2002) provided models of transit light curves derived from a simple two-body star-planet system. TAP can, thus, determine the best two-body orbital model from the observational data. In order to detect possible changes in orbital parameters, we analysed individual epochs separately.

Before using TAP, the target’s flux was normalized so that the out-of-transit flux values were close to unity. Moreover, as described in Eastman et al. (2010), TDB-based BJD was used for the time stamps in light curves here.

These light-curve data were then loaded into TAP to start MCMC chains. For each

light curve, five chains of length 300000 were computed. To start an MCMC chain in TAP, we needed to set the initial values of the following parameters: orbital period  $P$ , orbital inclination  $i$ , semi-major axis  $a$  (in the unit of stellar radius  $R_*$ ), the planet’s radius  $R_p$  (in the unit of stellar radius), the mid-transit time  $T_m$ , the linear limb darkening coefficient  $u_1$ , the quadratic limb darkening coefficient  $u_2$ , orbital eccentricity  $e$  and the longitude of periastron  $\omega$ . Once the above initial values were set, one could choose any one of the above to be: (1) completely fixed (2) completely free to vary or (3) varying following a Gaussian function, i.e. Gaussian prior, during the MCMC chain in TAP.

We analyzed each light curve through TAP separately and, thus, the orbital period was treated as a fixed parameter. The value of the orbital period in Sozzetti et al.(2009) was adopted. Because the orbital period is fixed, the semi-major axis shall not be completely free to vary. Thus, a Gaussian prior centred on the value 5.926 with  $\sigma = 0.056$  was set for  $a/R_*$  during TAP runs, where both the central value and the error bar were taken from Sozzetti et al.(2009).

Moreover,  $e$  and  $\omega$  are simply fixed to be zero, and  $i$  is treated in the same way as the semi-major axis. We leave the mid-transit times  $T_m$  and  $R_p/R_*$  to be completely free during TAP runs and obtain their best values for each light curve. They are the main parameters we would like to obtain through light-curve data.

Parameter	Initial Value	During MCMC Chains
$P$ (days)	1.30618581	fixed
$i$ (deg)	81.85	a Gaussian prior with $\sigma = 0.16$
$a/R_*$	5.926	a Gaussian prior with $\sigma = 0.056$
$R_p/R_*$	0.1655	free
$T_m$	set-by-eye	free
$u_1$	Claret (2000,2004)	a Gaussian prior with $\sigma = 0.05$
$u_2$	Claret (2000,2004)	a Gaussian prior with $\sigma = 0.05$
$e$	0.0	fixed
$\omega$	0.0	fixed

Table 2: The parameter setting. The initial values of  $P, i, a/R_*, R_p/R_*$  are set as the values in Sozzetti et al.(2009)

For the limb darkening effect, a quadratic limb darkening law with coefficients bi-linearly interpolated from Claret (2000, 2004) to the values effective temperature  $T_{\text{eff}} = 5650.0$  K, stellar surface gravity  $\log g = 4.40$  cm/s<sup>2</sup>, metallicity  $[M/H] = -0.2$  and micro-turbulent velocity  $V_t = 2.0$  km/s is adopted, as in Sozzetti et al. (2009). Thus, the limb darkening

coefficients are treated as prior parameters. However, Southworth (2008) found that the difference between the best fitted limb darkening coefficients and those theoretical values interpolated from Claret (2000, 2004) could be about 0.1 or 0.2. Thus, in order to take this possible difference into account, a Gaussian prior centred on the theoretical values with  $\sigma = 0.05$  is set for limb darkening coefficients  $u_1$  and  $u_2$  during TAP runs, where the value  $\sigma = 0.05$  is taken as half of 0.1 and could make the Gaussian distribution’s full width include possible differences. The details of parameter setting for TAP runs are listed in Table 2.

The limb darkening coefficients are dependent on the filters employed during observations. Table 3 lists these theoretical limb darkening coefficients  $u_1$  and  $u_2$  for all bands considered in this paper. In any TAP run, these theoretical values are used as the initial  $u_1$  and  $u_2$ , and also as the central values of Gaussian priors. However, the nine RISE light curves in Gibson et al. (2009) were obtained through a special instrument with a single non-standard wide-band filter covering V and R bands. The average values for filters V and R in Table 3 were used as the theoretical limb darkening coefficients  $u_1$  and  $u_2$  when we ran TAP for these light curves. Moreover, in Colon et al. (2010), two narrow near-infrared bands at 790.2 nm and 794.4 nm are used to obtain high-precision transit data. There are 36 data points at 790.2 nm and 35 data points at 794.4 nm, so in total 71 data points are used for one transit event. Since these two wavelengths are very close and are at the centre of I band, the  $u_1$  and  $u_2$  for Filter I, shown in Table 3, were used as the theoretical limb darkening coefficients.

filter	$u_1$	$u_2$
B	0.6379	0.1792
V	0.4378	0.2933
R	0.3404	0.3190
I	0.2576	0.3186
sloan u	0.8112	0.0554
sloan g	0.5535	0.2351
sloan r	0.3643	0.3178
sloan i	0.2777	0.3191
sloan z	0.2179	0.3162

Table 3: The theoretical limb darkening coefficients for the TrES-3 star.

All results derived through TAP are shown in Tables 4 and 5. The first TrES-3 transit in Sozzetti et al.(2009) is defined as epoch  $E = 0$ , and other transits’ epochs are defined accordingly. These two tables list all parameter values with uncertainties following the order

of epochs. Moreover, the observational light curves and best fitting models of our own data are presented in Figure 1, where the points are observational data and solid curves are the best fitting models. The original data points in Figure 1 are available in a machine-readable form in the electronic version of Table 6.

Epoch	Data Source	$T_m$	$i$ (deg)	$a/R_*$
0	(a)	4185.911111 <sup>+0.00021</sup> <sub>-0.00021</sub>	81.90 <sup>+0.10</sup> <sub>-0.11</sub>	5.906 <sup>+0.044</sup> <sub>-0.043</sub>
10	(a)	4198.97359 <sup>+0.00057</sup> <sub>-0.00066</sub>	81.79 <sup>+0.14</sup> <sub>-0.14</sub>	5.944 <sup>+0.052</sup> <sub>-0.052</sub>
22	(a)	4214.64695 <sup>+0.00032</sup> <sub>-0.00036</sub>	81.81 <sup>+0.12</sup> <sub>-0.12</sub>	5.915 <sup>+0.046</sup> <sub>-0.045</sub>
23	(a)	4215.95288 <sup>+0.00033</sup> <sub>-0.00031</sub>	81.77 <sup>+0.12</sup> <sub>-0.13</sub>	5.937 <sup>+0.047</sup> <sub>-0.047</sub>
267	(b)	4534.66317 <sup>+0.00019</sup> <sub>-0.00019</sub>	81.79 <sup>+0.12</sup> <sub>-0.12</sub>	5.952 <sup>+0.044</sup> <sub>-0.044</sub>
268	(a)	4535.96903 <sup>+0.00039</sup> <sub>-0.00037</sub>	81.83 <sup>+0.12</sup> <sub>-0.12</sub>	5.920 <sup>+0.048</sup> <sub>-0.047</sub>
281	(a)	4552.94962 <sup>+0.00020</sup> <sub>-0.00022</sub>	81.86 <sup>+0.11</sup> <sub>-0.11</sub>	5.939 <sup>+0.043</sup> <sub>-0.043</sub>
294	(a)	4569.92982 <sup>+0.00039</sup> <sub>-0.00040</sub>	81.82 <sup>+0.12</sup> <sub>-0.12</sub>	5.926 <sup>+0.047</sup> <sub>-0.047</sub>
313	(a)	4594.74682 <sup>+0.00037</sup> <sub>-0.00034</sub>	81.85 <sup>+0.12</sup> <sub>-0.13</sub>	5.943 <sup>+0.047</sup> <sub>-0.047</sub>
329	(b)	4615.64621 <sup>+0.00020</sup> <sub>-0.00021</sub>	81.81 <sup>+0.11</sup> <sub>-0.11</sub>	5.915 <sup>+0.044</sup> <sub>-0.044</sub>
342	(b)	4632.62690 <sup>+0.00020</sup> <sub>-0.00019</sub>	81.81 <sup>+0.11</sup> <sub>-0.11</sub>	5.937 <sup>+0.042</sup> <sub>-0.042</sub>
355	(b)	4649.60712 <sup>+0.00019</sup> <sub>-0.00017</sub>	81.81 <sup>+0.11</sup> <sub>-0.11</sub>	5.931 <sup>+0.042</sup> <sub>-0.041</sub>
358	(b)	4653.52661 <sup>+0.00091</sup> <sub>-0.00092</sub>	81.89 <sup>+0.14</sup> <sub>-0.15</sub>	5.913 <sup>+0.052</sup> <sub>-0.052</sub>
365	(b)	4662.66984 <sup>+0.00059</sup> <sub>-0.00060</sub>	81.90 <sup>+0.13</sup> <sub>-0.14</sub>	5.915 <sup>+0.051</sup> <sub>-0.052</sub>
371	(b)	4670.50709 <sup>+0.00034</sup> <sub>-0.00034</sub>	81.86 <sup>+0.11</sup> <sub>-0.11</sub>	5.885 <sup>+0.046</sup> <sub>-0.045</sub>
374	(b)	4674.42521 <sup>+0.00028</sup> <sub>-0.00028</sub>	81.74 <sup>+0.11</sup> <sub>-0.12</sub>	5.965 <sup>+0.047</sup> <sub>-0.045</sub>
381	(b)	4683.56812 <sup>+0.00042</sup> <sub>-0.00041</sub>	81.85 <sup>+0.12</sup> <sub>-0.13</sub>	5.927 <sup>+0.048</sup> <sub>-0.048</sub>
665	(c)	5054.52523 <sup>+0.00018</sup> <sub>-0.00017</sub>	81.83 <sup>+0.10</sup> <sub>-0.11</sub>	5.932 <sup>+0.043</sup> <sub>-0.043</sub>
885	(d)	5341.8838 <sup>+0.0011</sup> <sub>-0.0010</sub>	81.81 <sup>+0.15</sup> <sub>-0.15</sub>	5.935 <sup>+0.053</sup> <sub>-0.053</sub>
898	(d)	5358.86606 <sup>+0.00076</sup> <sub>-0.00074</sub>	81.75 <sup>+0.14</sup> <sub>-0.14</sub>	5.957 <sup>+0.053</sup> <sub>-0.052</sub>
901	(d)	5362.7847 <sup>+0.0011</sup> <sub>-0.00098</sub>	81.83 <sup>+0.15</sup> <sub>-0.15</sub>	5.937 <sup>+0.053</sup> <sub>-0.053</sub>
904	(d)	5366.70215 <sup>+0.00080</sup> <sub>-0.00077</sub>	81.95 <sup>+0.14</sup> <sub>-0.15</sub>	5.987 <sup>+0.052</sup> <sub>-0.052</sub>
911	(d)	5375.84617 <sup>+0.00089</sup> <sub>-0.00090</sub>	81.89 <sup>+0.14</sup> <sub>-0.15</sub>	5.912 <sup>+0.052</sup> <sub>-0.052</sub>

Table 4: The results of light-curve analysis for  $T_m$ ,  $i$ , and  $a/R_*$ . Data sources: (a) Sozzetti et al.(2009), (b) Gibson et al. (2009), (c) Colon et al. (2010), and (d) this work. To save space, the value of the mid-transit time  $T_m$  (in TDB-based BJD) is subtracted by 2450000.

For a photometric light curve, there are two possible sources of error. The uncorrelated Gaussian scatter is called “white noise”, and the time correlated Gaussian scatter is “red noise”. TAP is designed to decompose and model the above two sources of error with the

Epoch	$R_p/R_*$	$\mu_1$	$\mu_2$
0	0.1656 <sup>+0.0026</sup> <sub>-0.0022</sub>	0.219 <sup>+0.049</sup> <sub>-0.048</sub>	0.317 <sup>+0.050</sup> <sub>-0.049</sub>
10	0.1734 <sup>+0.0075</sup> <sub>-0.0068</sub>	0.642 <sup>+0.049</sup> <sub>-0.049</sub>	0.183 <sup>+0.049</sup> <sub>-0.049</sub>
22	0.1708 <sup>+0.0049</sup> <sub>-0.0040</sub>	0.440 <sup>+0.049</sup> <sub>-0.048</sub>	0.292 <sup>+0.049</sup> <sub>-0.049</sub>
23	0.1716 <sup>+0.0058</sup> <sub>-0.0049</sub>	0.563 <sup>+0.049</sup> <sub>-0.049</sub>	0.242 <sup>+0.048</sup> <sub>-0.049</sub>
267	0.1691 <sup>+0.0041</sup> <sub>-0.0034</sub>	0.393 <sup>+0.050</sup> <sub>-0.050</sub>	0.312 <sup>+0.050</sup> <sub>-0.050</sub>
268	0.1639 <sup>+0.0046</sup> <sub>-0.0039</sub>	0.283 <sup>+0.050</sup> <sub>-0.049</sub>	0.322 <sup>+0.049</sup> <sub>-0.049</sub>
281	0.1634 <sup>+0.0033</sup> <sub>-0.0027</sub>	0.350 <sup>+0.049</sup> <sub>-0.049</sub>	0.308 <sup>+0.050</sup> <sub>-0.050</sub>
294	0.1648 <sup>+0.0059</sup> <sub>-0.0052</sub>	0.275 <sup>+0.049</sup> <sub>-0.049</sub>	0.317 <sup>+0.050</sup> <sub>-0.050</sub>
313	0.1646 <sup>+0.0053</sup> <sub>-0.0046</sub>	0.273 <sup>+0.050</sup> <sub>-0.049</sub>	0.317 <sup>+0.050</sup> <sub>-0.050</sub>
329	0.1674 <sup>+0.0033</sup> <sub>-0.0028</sub>	0.400 <sup>+0.049</sup> <sub>-0.050</sub>	0.313 <sup>+0.049</sup> <sub>-0.049</sub>
342	0.1685 <sup>+0.0036</sup> <sub>-0.0031</sub>	0.390 <sup>+0.048</sup> <sub>-0.048</sub>	0.307 <sup>+0.049</sup> <sub>-0.049</sub>
355	0.1649 <sup>+0.0030</sup> <sub>-0.0026</sub>	0.381 <sup>+0.048</sup> <sub>-0.049</sub>	0.297 <sup>+0.049</sup> <sub>-0.049</sub>
358	0.1676 <sup>+0.0084</sup> <sub>-0.0074</sub>	0.385 <sup>+0.049</sup> <sub>-0.049</sub>	0.302 <sup>+0.050</sup> <sub>-0.049</sub>
365	0.1664 <sup>+0.0071</sup> <sub>-0.0061</sub>	0.386 <sup>+0.049</sup> <sub>-0.049</sub>	0.303 <sup>+0.049</sup> <sub>-0.049</sub>
371	0.1619 <sup>+0.0032</sup> <sub>-0.0029</sub>	0.393 <sup>+0.048</sup> <sub>-0.049</sub>	0.305 <sup>+0.049</sup> <sub>-0.048</sub>
374	0.1616 <sup>+0.0041</sup> <sub>-0.0037</sub>	0.390 <sup>+0.049</sup> <sub>-0.049</sub>	0.308 <sup>+0.049</sup> <sub>-0.049</sub>
381	0.1644 <sup>+0.0053</sup> <sub>-0.0044</sub>	0.387 <sup>+0.050</sup> <sub>-0.049</sub>	0.305 <sup>+0.049</sup> <sub>-0.050</sub>
665	0.1655 <sup>+0.0026</sup> <sub>-0.0023</sub>	0.260 <sup>+0.049</sup> <sub>-0.049</sub>	0.320 <sup>+0.049</sup> <sub>-0.049</sub>
885	0.1683 <sup>+0.0097</sup> <sub>-0.0086</sub>	0.345 <sup>+0.050</sup> <sub>-0.050</sub>	0.323 <sup>+0.050</sup> <sub>-0.050</sub>
898	0.1627 <sup>+0.0094</sup> <sub>-0.0086</sub>	0.345 <sup>+0.050</sup> <sub>-0.050</sub>	0.324 <sup>+0.050</sup> <sub>-0.050</sub>
901	0.160 <sup>+0.011</sup> <sub>-0.011</sub>	0.341 <sup>+0.050</sup> <sub>-0.049</sub>	0.320 <sup>+0.050</sup> <sub>-0.050</sub>
904	0.1646 <sup>+0.0077</sup> <sub>-0.0067</sub>	0.334 <sup>+0.050</sup> <sub>-0.050</sub>	0.296 <sup>+0.050</sup> <sub>-0.050</sub>
911	0.1543 <sup>+0.0086</sup> <sub>-0.0074</sub>	0.338 <sup>+0.050</sup> <sub>-0.049</sub>	0.316 <sup>+0.050</sup> <sub>-0.050</sub>

Table 5: The results of light-curve analysis for parameters  $R_p/R_*$ ,  $\mu_1$  and  $\mu_2$ .

technique of wavelet analysis.

The error bars of orbital parameters and mid-transit times shown in Table 4 are the results of our TAP runs. There are five chains in each of our TAP runs, and all of the chains are added together into the final results. The 15.9, 50.0 and 84.1 percentile levels are recorded. The 50.0 percentile, i.e., median level, is used as the best value, and the other two percentile levels give the error bar.

This error analysis was tested and shown to be successful in Gazak et al. (2011). Moreover, we found that when the deviations of transit-light-curve data are smaller, the resulting error bars become smaller. Thus, the error bar does reflect the quality of data.

UT Date	TDB-based BJD	Relative Flux
2010 May 25	2455341.781604507	0.996660
	2455341.783375395	1.003077
	2455341.785134680	0.998439
2010 Jun 11	2455358.803032950	0.998805
	2455358.804803775	1.002478
	2455358.806563056	0.997858
2010 Jun 15	2455362.720387560	0.999725
	2455362.722158398	1.003418
	2455362.723940820	1.006198
2010 Jun 19	2455366.657799268	0.998268
	2455366.659570101	0.997392
	2455366.661329362	1.001116
2010 Jun 28	2455375.782958203	0.997703
	2455375.784729044	0.999569
	2455375.786499864	0.999101

Table 6: The photometric light-curve data of this work. This table is available in its entirety in the on-line journal. A portion is shown here for guidance.

The MCMC procedure in TAP gives a reasonable estimation on the error related to the data itself. Therefore, the error bars we obtained here should have been consistent with the scattering and quality of the light curves, and provide reliable error estimates.

#### 4. Comparison with Previous Studies

Gibson et al. (2009) presented the results of transit timing residuals in their Figure 3, where both the data in Gibson et al. (2009) and Sozzetti et al. (2009) are included. Tables 3 and 4 in Gibson et al. (2009) provide the values of mid-transit times in HJD for all their nine transit light curves and also for those eight light curves from Sozzetti et al. (2009). After converting these values from HJD to TDB-based BJD and adopting their values of uncertainties, an ephemeris is calculated by minimizing  $\chi^2$  through fitting a linear function:

$$T_m^C(E) = PE + T_m^C(0), \quad (1)$$

where  $P$  is the orbital period,  $E$  is an epoch,  $T_m^C(E)$  is the calculated mid-transit time at a given epoch  $E$ , and so  $T_m^C(0)$  is the value for  $E = 0$ . We found that  $P = 1.30618631 \pm$

0.00000016,  $T_m^C(0) = 2454185.91111514 \pm 0.00005033$ , and the corresponding  $\chi^2 = 34.26$ . Since the degree of freedom is 15, the reduced  $\chi^2 = 2.28$ . The  $O - C$  diagram, which shows the differences between the observational mid-transit time and the calculated mid-transit time of a simple two-body star-planet system (i.e.  $T_m - T_m^C$ ) as a function of epoch  $E$ , is shown in the top panel of Figure 2.

On the other hand, as we mentioned in §3, we also have the mid-transit times directly derived from the light curves in the study of Sozzetti et al.(2009) and Gibson et al.(2009) as shown in Table 4. Similarly, by minimizing  $\chi^2$  through fitting a linear function as Eq.(1), it was found that  $P = 1.30618691 \pm 0.00000051$ ,  $T_m^C(0) = 2454185.91099199 \pm 0.00015123$ , and the corresponding  $\chi^2 = 19.69$ . As the degree of freedom is 15, the reduced  $\chi^2 = 1.31$ . Thus, another  $O - C$  diagram can be plotted as in the bottom panel of Figure 2.

From both panels in Figure 2 and the resulting ephemeris, we see that what we derived directly from light curves is correct. Our error bars are larger than those in the previous work, so that the value of  $\chi^2$  is smaller. Therefore, the error bars are unlikely to be underestimated in our results presented in this paper.

## 5. Transit Timing Variations

### 5.1. A New Ephemeris

When 23 light curves mentioned in §2 are all considered, we would get a new ephemeris by minimizing  $\chi^2$  through fitting a linear function as Eq.(1). We find that  $P = 1.30618619 \pm 0.00000015 = P_l \pm 0.00000015$ , where  $P_l \equiv 1.30618619$ ,  $T_m^C(0) = 2454185.91116430 \pm 0.00006123 = T_l \pm 0.00006123$ , where  $T_l \equiv 2454185.91116430$ , and the corresponding  $\chi^2 = 31.95$ . Because the degree of freedom is 21, the reduced  $\chi^2 = 1.52$ . Using this new ephemeris, the  $O - C$  diagram is shown in Figure 3.

Therefore, for a straight line fit, i.e. a null-TTV model, our reduced  $\chi^2$  with all considered 23 light curves is smaller than the value of 2.34 from Gibson et al. (2009). This could be partially due to error bars here being slightly larger than those in Gibson et al. (2009). Therefore, our error bars are not underestimated, and unlikely to lead to a result with false-positive TTVs.

## 5.2. The Frequency Analysis and Possible Models

In order to investigate whether there is any TTV, Lomb’s normalized periodogram (Press et al. 1992) was used to search for possible variations in the data. Figure 4 shows the resulting spectral power as a function of frequencies. We defined the frequency with largest power as  $f_1$ , i.e.  $f_1 \equiv 0.01055$ , and tested the possible TTVs with frequency  $f_1$  by minimizing  $\chi^2$  through fitting a function as:

$$T_S(E) = PE + b + a \sin(2\pi f_1 E - \phi_1), \quad (2)$$

where  $T_S(E)$  is the predicted mid-transit time at a given epoch  $E$ ,  $b, a, \phi_1$  are fitting parameters. We obtained that  $P = 1.30618631 \pm 0.00000031$ ,  $b = 2454185.91100290 \pm 0.00012187$ ,  $a = 0.00036500 \pm 0.00009570$  and  $\phi_1 = 3.97482109 \pm 0.25632765$ . The corresponding  $\chi^2 = 17.59$ . Since the degree of freedom is 19, the reduced  $\chi^2 = 0.93$ . Using the above best fitted parameters for  $T_S(E)$  and the new ephemeris  $P_l, T_l$  for  $T_m^C(E)$ , the curve  $T_S(E) - T_m^C(E)$  as a function of epoch  $E$  is plotted in the  $O - C$  diagram, together with data points, as shown in Figure 5.

In order to test the models with multiple frequencies, the frequency with the  $i$ -th highest power is defined as  $f_i$ , where  $i = 2, \dots, 5$ . Then, possible TTV models with  $N$  frequencies can be tested by minimizing  $\chi^2$  through fitting a function as:

$$T_S(E) = PE + b + a \prod_{i=1}^N \sin(2\pi f_i E - \phi_i), \quad (3)$$

where  $N = 2, \dots, 5$ . These results of multiple frequencies, together with the results of null-TTV and one-frequency TTV models, are all summarized in Table 7. Similarly, employing the best fitted parameters for  $T_S(E)$  and the new ephemeris  $P_l, T_l$  for  $T_m^C(E)$ , the curves  $T_S(E) - T_m^C(E)$  as a function of epoch  $E$  are shown in the  $O - C$  diagram, together with data points, as in Figure 6(A)-(D).

From the values of reduced  $\chi^2$  presented in Table 7, it is clear that the model with one frequency, i.e. 1-frequency model, has the highest probability to produce the possible TTVs implied by the observational data. In fact, 1-frequency, 2-frequency, 3-frequency and 4-frequency models are all better than the null-TTV model as their reduced  $\chi^2$  are closer to unity. Among these, the curve of 3-frequency model almost goes through the error bars of all points. Due to the over-fitting, the reduced  $\chi^2$  of 5-frequency model is very small.

## 6. Concluding Remarks

In this paper, five new transit light curves and others from the literature, including one from Colon et al. (2010), eight from Sozzetti et al. (2009) and another nine from Gibson et

al. (2009), are employed to obtain the orbital parameters of the TrES-3 planetary system. These 23 transit light curves, which cover an overall timescale of 911 epochs, have been analyzed through a self-consistent standard procedure, so that the possible TTVs could be investigated carefully. We found that a null transit-timing-variation produced a fit with a reduced  $\chi^2=1.52$ . This result agrees with the conclusions in previous work that the transit timing variations might not exist in these data.

On the other hand, we also found that a 1-frequency transit-timing-variation model which gives a fit with a reduced  $\chi^2=0.93$ . Thus, this interesting model is statistically more probable than the one with null TTVs. We conclude that the future high-precision observations and further dynamical work for this planetary system will lead to fruitful scientific results.

### Acknowledgment

The authors would like to thank the referee for good suggestions which greatly improved this paper. The authors are grateful to N.P. Gibson for kindly providing the RISE light-curve data from Gibson et al. (2009), and A. Kong for the telescope time. This work was supported in part by the National Science Council, Taiwan, under NSC 98-2112-M-007-006-MY2 and NSC 100-2112-M-007-003-MY3. PT gratefully acknowledges the support from the Inter-University Centre for Astronomy and Astrophysics (IUCAA), Pune, India, under the Associateship Programme. J.J.H. acknowledges support by the National Natural Science Foundation of China (Grants No. 11273068, 10973044, 10833001), the Natural Science Foundation of Jiangsu Province (Grant No. BK2009341), the Foundation of Minor Planets of Purple Mountain Observatory, and the innovative and interdisciplinary program by CAS (Grant No. KJZD-EW-Z001).

### REFERENCES

- Agol, E., Steffen, J., Sari, R., Clarkson, W. 2005 MNRAS, 359, 567
- Claret, A. 2000, A&A, 363, 1081
- Claret, A. 2004, A&A, 428, 1001
- Colon, K. D. et al. 2010, MNRAS, 408, 1494
- Eastman, J., Siverd, R., Gaudi, B. S. 2010, PASP, 122, 935

- Fressin, F. et al. 2010, ApJ, 711, 374
- Fulton, B. J. et al. 2011, AJ, 142, 84
- Gazak, J. Z., Johnson, J. A., Tonry, J., Eastman, J., Mann, A. W., Agol, E. 2011, arXiv:1102.1036
- Gibson, N. P. et al. 2009, ApJ, 700, 1078
- Holman, M. J., Murray, N. W. 2005, Science, 307, 1288
- Holman, M. J. et al. 2010, Science, 330, 51
- Lee, J. W. et al. 2011, PASJ, 63, 301
- Lissauer, J. J. et al. 2011, Nature, 470, 53
- Maciejewski, G. et al. 2010, MNRAS, 407, 2625
- Mandel, K., Agol, E. 2002, ApJ, 580, L171
- Miller-Ricci, E. et al. 2008, ApJ, 682, 586
- O’Donovan, F. T. et al. 2007, ApJ, 663, L37
- Press, W. H. et al. 1992, Numerical Recipes in Fortran, Cambridge University Press
- Sozzetti, A. et al. 2009, ApJ, 691, 1145
- Southworth, J. 2008, MNRAS, 386, 1644
- Winn, J. N. et al. 2009, AJ, 137, 3826

Model	Fitted Parameters	Degree of Freedom	Reduced $\chi^2$
null-TTV	$P = 1.30618619 \pm 0.00000015$ $T_m^C(0) = 2454185.91116430 \pm 0.00006123$	21	1.52
1-frequency	$P = 1.30618631 \pm 0.00000031$ $b = 2454185.91100290 \pm 0.00012187$ $a = 0.00036500 \pm 0.00009570$ $\phi_1 = 3.97482109 \pm 0.25632765$	19	0.93
2-frequency	$P = 1.30618560 \pm 0.00000045$ $b = 2454185.91144686 \pm 0.00016052$ $a = 0.00053559 \pm 0.00018953$ $\phi_1 = 2.46731638 \pm 0.28913521$ $\phi_2 = 5.58758211 \pm 0.31948870$	18	1.32
3-frequency	$P = 1.30618619 \pm 0.00000031$ $b = 2454185.91111750 \pm 0.00013402$ $a = 0.00218541 \pm 0.00062400$ $\phi_1 = 0.49000000 \pm 0.30458730$ $\phi_2 = 2.39100003 \pm 0.13629963$ $\phi_3 = 0.01779999 \pm 0.07340797$	17	0.85
4-frequency	$P = 1.30618572 \pm 0.00000036$ $b = 2454185.91134611 \pm 0.00018133$ $a = 0.00142777 \pm 0.00059381$ $\phi_1 = 3.72499990 \pm 0.31523481$ $\phi_2 = 2.39299988 \pm 0.42470514$ $\phi_3 = 2.48769998 \pm 0.42087095$ $\phi_4 = 0.27669999 \pm 0.28758257$	16	0.86
5-frequency	$P = 1.30618596 \pm 0.00000040$ $b = 2454185.91131390 \pm 0.00014342$ $a = -0.00219894 \pm 0.00088575$ $\phi_1 = 3.68168663 \pm 0.36549767$ $\phi_2 = 0.23282741 \pm 0.14959095$ $\phi_3 = 5.53840208 \pm 0.35394611$ $\phi_4 = 2.04802298 \pm 0.34912726$ $\phi_5 = 4.09944820 \pm 0.33490377$	15	0.64

Table 7: The values of fitted parameters, degree of freedom, reduced  $\chi^2$  of the null-TTV model and  $i$ -frequency models, where  $i=1,2,\dots,5$ .

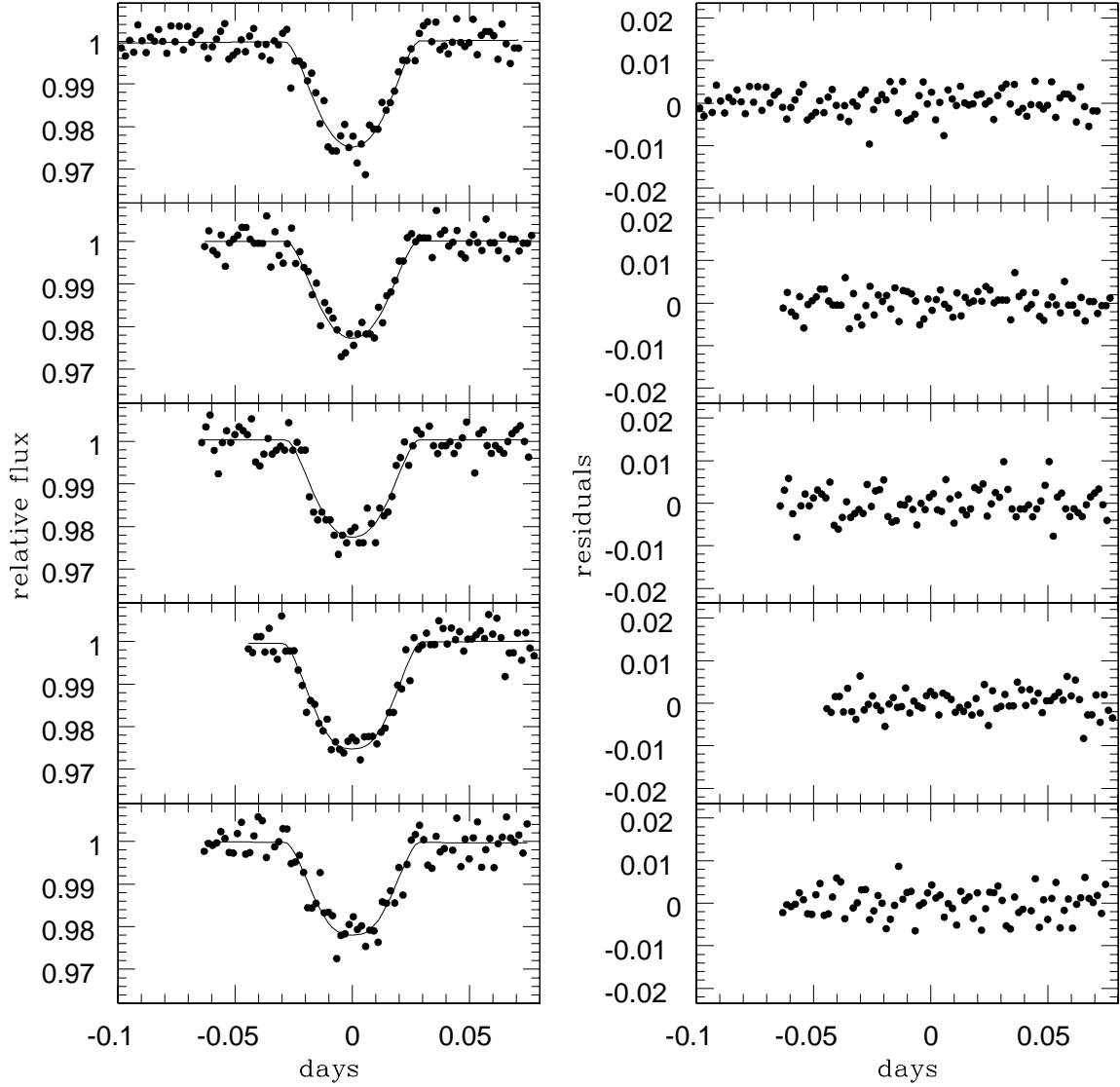


Fig. 1.— (Left panels) The normalized relative flux as a function of the time (the offset from mid transit time and in TDB-based BJD) of five transit light curves of this work: points are the data and curves are models. (Right panels) The corresponding residuals. From top to bottom: our observational data of Run 1-5 listed in Table 1.

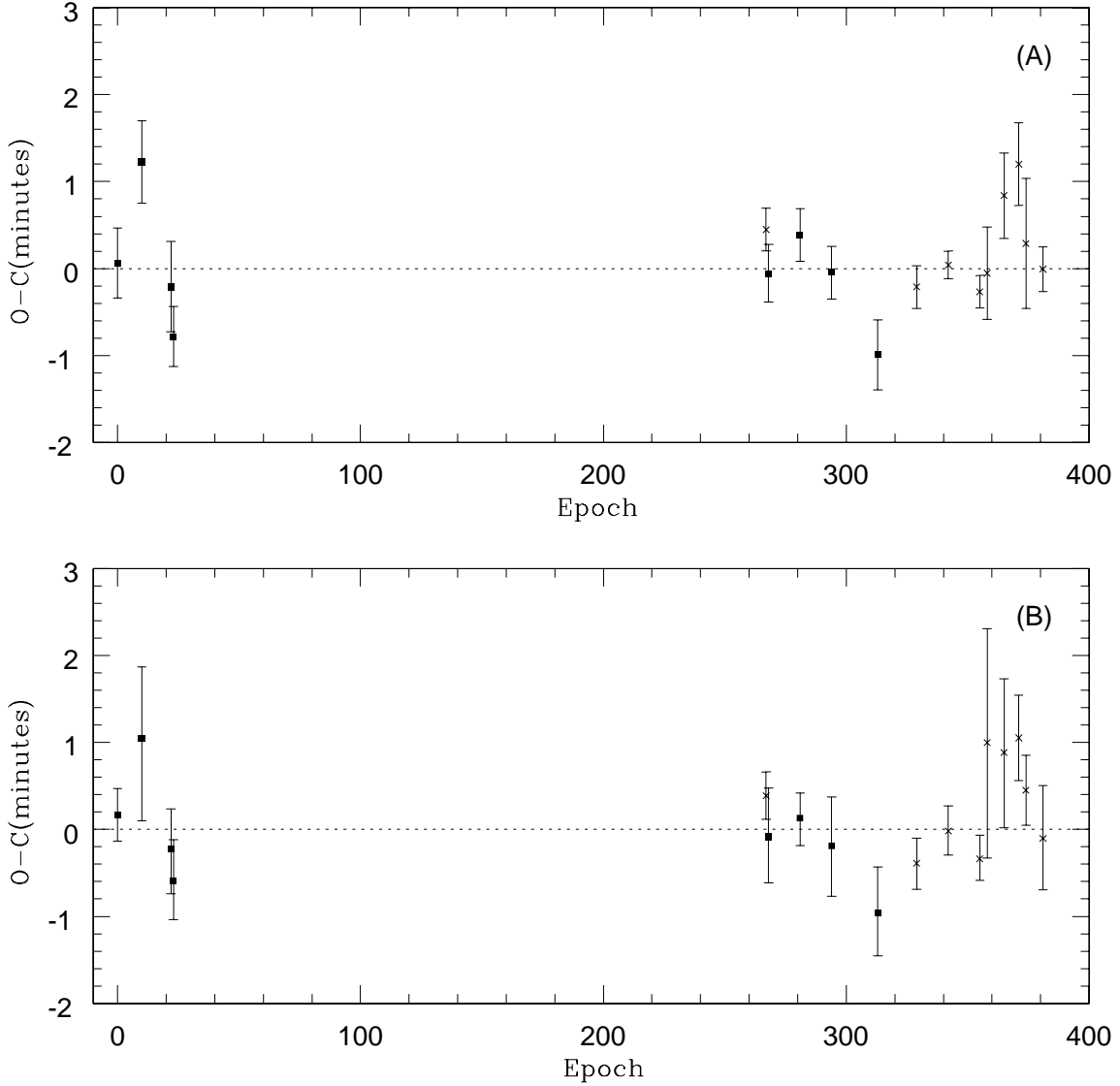


Fig. 2.— The  $O - C$  diagram. Panel (A) is for the results in which mid-transit times are taken from Table 3 and Table 4 of Gibson et al. (2009) and converted to be in TDB-based BJD. Panel (B) is for the results of our analysis as those listed in Table 4 but only those from Data Source (a) and (b) are included here. Squares are for the data from Sozzetti et al (2009), and crosses are for Gibson et al. (2009).

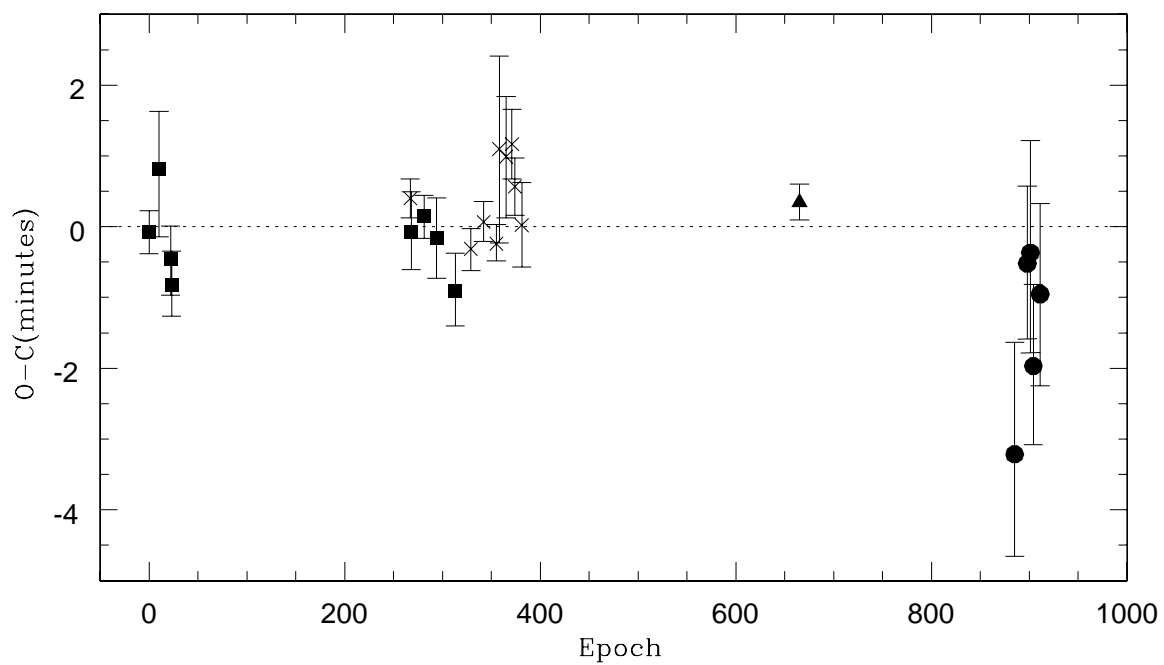


Fig. 3.— The  $O - C$  diagram for all results shown in Table 4. The full circles are for this work, squares are for the data from Sozzetti et al (2009), the full triangle is for 10.4 meter GTC data, and crosses are for the data from Gibson et al. (2009).

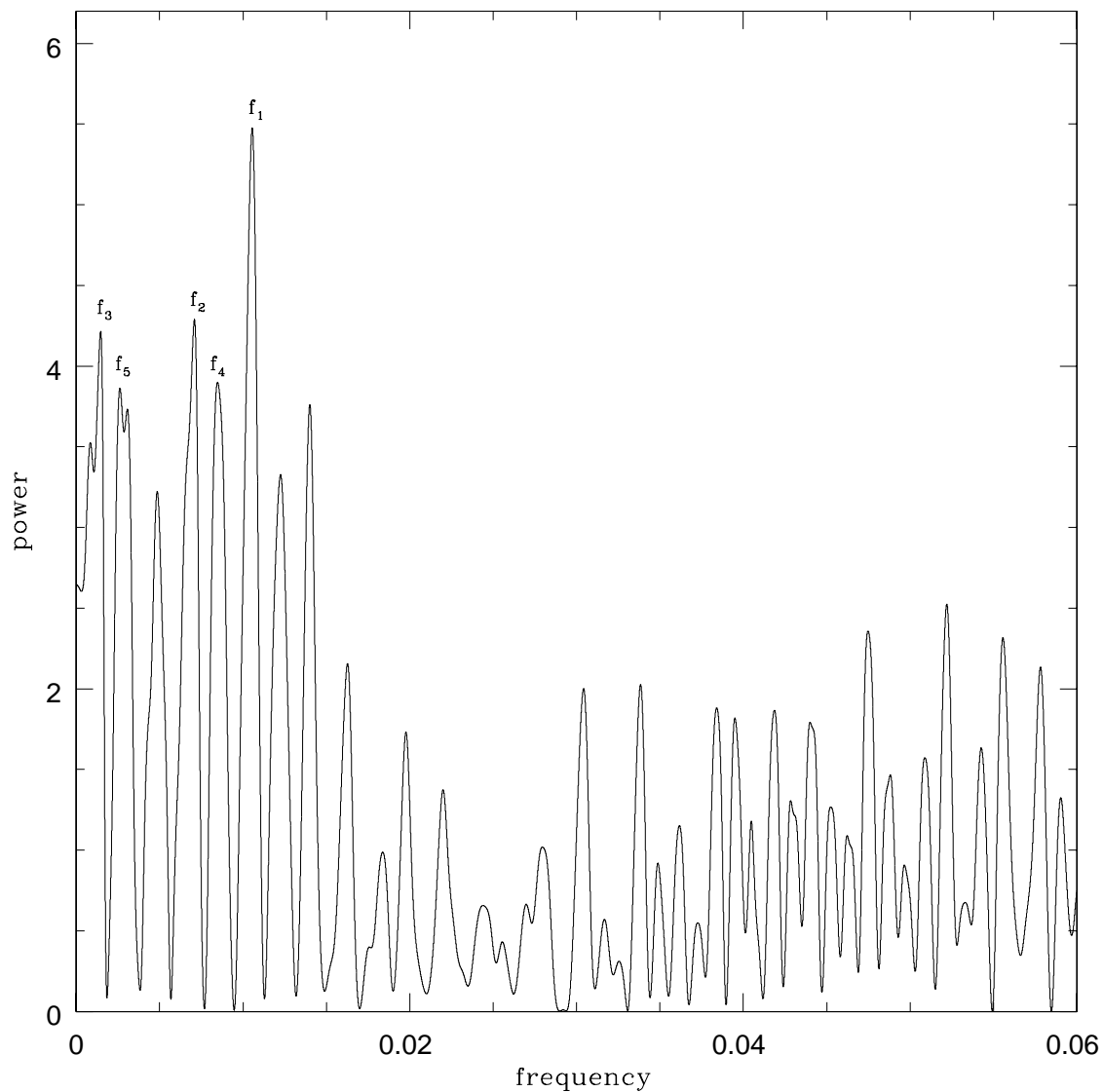


Fig. 4.— The spectral power as a function of frequencies for the data points shown in Figure 3. The top five frequencies are marked as  $f_1, f_2, f_3, f_4$  and  $f_5$ .

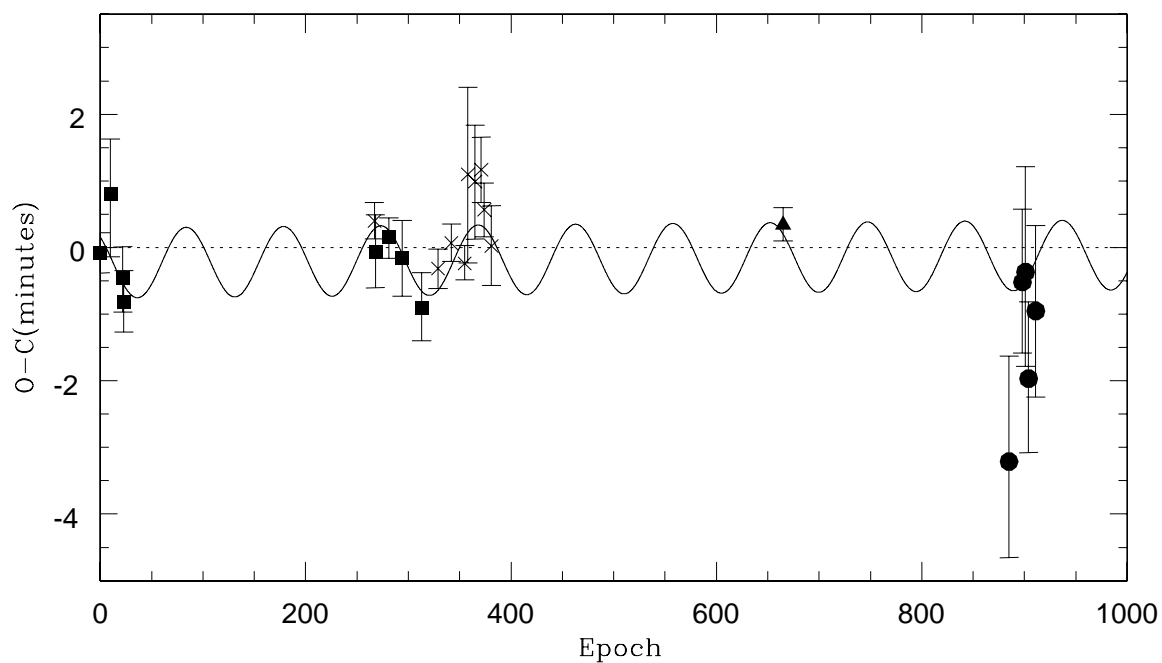


Fig. 5.— The 1-frequency model and the  $O-C$  diagram. The curve is for the fitting function. The full circles are for this work, squares are for the data from Sozzetti et al (2009), the full triangle is for 10.4 meter GTC data, and crosses are for the data from Gibson et al.(2009).

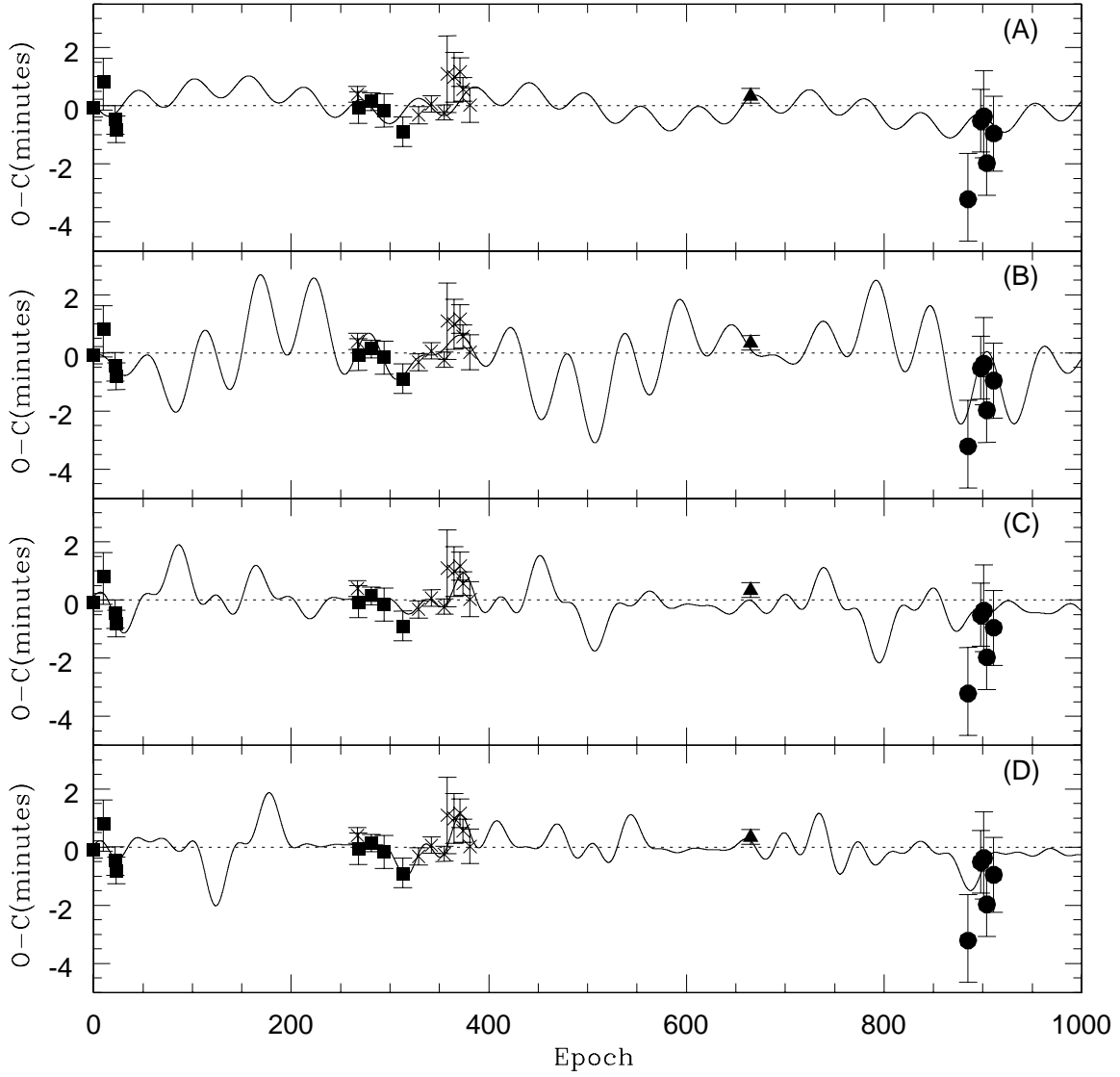


Fig. 6.— The  $i$ -frequency model and the  $O - C$  diagram, where  $i=2,3,4,5$  (Panel (A)-(D)). The curve is for the fitting function. The full circles are for this work, squares are for the data from Sozzetti et al (2009), the full triangle is for 10.4 meter GTC data, and crosses are for the data from Gibson et al.(2009).